Reconstruction of 3D Surface Maps from Anterior Segment Optical Coherence Tomography Images Using Graph Theory and Genetic Algorithms

Dominic Williams[a,b], Yalin Zheng[b], Pinakin Gunvant Davey[c], Fangjun Bao[d], Meixiao Shen[d] and Ahmed Elsheikh[a,e]

[a] Ocular Biomechanics and Biomaterials Group, School of Engineering, University of Liverpool , UK
[b] Department of Eye and Vision Science, University of Liverpool, UK
[c] College of Optometry, Western University of Health Sciences, CA, USA
[d] School of Optometry and Ophthalmology and Eye Hospital, Wenzhou Medical University, Zhejiang Province, China
[e] NIHR Biomedical Research Centre for Ophthalmology, Moorfields Eye Hospital NHS Foundation Trust and UCL Institute of Ophthalmology, UK

Dominic Williams
School of Engineering
The Quadrangle
The University of Liverpool
Brownlow Hill
Liverpool
L69 3GH
dominic.williams@liv.ac.uk

Yalin Zheng
Department of Eye and Vision Science
Institute of Ageing and Chronic Disease
3rd Floor, UCD Building
Daulby Street
Liverpool
L69 3GA
yalin.zheng@liv.ac.uk

Pinakin Gunvant Davey
Pomona, CA campus
309 E. Second St.
Pomona, CA 91766-1854

Fangjun Bao
Eye Hospital
Wenzhou Medical University
No. 270, Xueyuanxi Road
Wenzhou City
Zhejiang Province
325027
China
bfjmd@126.com

Meixiao Shen
Eye Hospital
Wenzhou Medical University
No. 270, Xueyuanxi Road
Wenzhou City

Zhejiang Province
325027
China
shenmxiao7@hotmail.com

Ahmed Elsheikh
School of Engineering
The Quadrangle
The University of Liverpool
Brownlow Hill
Liverpool
L69 3GH
elsheikh@liverpool.ac.uk

***Abstract*— Automatic segmentation of anterior segment optical coherence tomography images provides an important tool to aid management of ocular diseases. Previous studies have mainly focused on 2D segmentation of these images. A novel technique capable of producing 3D maps of the anterior segment is presented here. This method uses graph theory and dynamic programming with shape constraint to segment the anterior and posterior surfaces in individual 2D images. Genetic algorithms are then used to align 2D images to produce a full 3D representation of the anterior segment. In order to validate the results of the 2D segmentation comparison is made to manual segmentation over a set of 39 images. For the 3D reconstruction a data set of 17 eyes is used. These have each been imaged twice so a repeatability measurement can be made. Good agreement was found with manual segmentation for the 2D segmentation method achieving a Dice similarity coefficient of 0.96, which is comparable to the inter-observer agreement. Good repeatability of results was demonstrated with the 3D registration method. A mean difference of 1.77 pixels was found between the anterior surfaces found from repeated scans of the same eye.**

***Index Terms*— optical coherence tomography (OCT), anterior segment, cornea, dynamic programming (DP), graph cut and genetic algorithms (GA)**

1. INTRODUCTION

OPTICAL coherence tomography (OCT) is capable of producing high resolution images of the human eye. These images are extensively used for diagnostics looking at the posterior segment of the eye (Swanson et al., 1993). OCT images of the anterior segment have also been used in several medical applications including contact lens fitting, ectasia diagnosis, surgical planning and monitoring of patients with eye pathologies (Hall et al., 2011; Kaluzy et al., 2006; Konstantopoulos et al., 2008; Sakata et al., 2008). One of the challenges faced is the automated segmentation of anterior segment images.

Commercially available OCT devices have different inbuilt segmentation methods. Currently only CASIA (Tomey, Tokyo, Japan) is able to both image and automatically segment the entire anterior segment (Liu et al., 2011). However, we do not know the proprietary details of the segmentation approach used. The use of proprietary software only coming with the device will also limit the access for many applications. Other commercially available devices are either limited to only imaging a small section of the cornea or are unable to automatically segment the entire anterior segment like the Visante OCT system (Zeiss Meditec Inc., Dublin, California) (Reinstein et al., 2012). Previous segmentation techniques have used a variety of techniques to achieve results but have mainly focused on 2D segmentation only (LaRocca et al., 2011; Shen et al., 2011; Tian et al., 2011; Williams et al., 2013, 2015).

2D segmentation techniques of the anterior segment have included those that use threshold methods (Shen et al., 2011), level set based techniques (Williams et al., 2013), graph cut techniques (Williams et al., 2015) and dynamic programming (LaRocca et al., 2011). La Rocca et al. used graph theory and dynamic programming for the segmentation of spectral domain OCT (SD OCT) images [10]. These images only included the central region of the cornea. The method used the image gradient to identify edges on the images; Dijkstra's algorithm (Dijkstra, 1959) was then used to find the shortest path through the image based on the image gradient. Three boundaries on the cornea to be segmented; their results were in good agreement with manual observers. The central corneal region covered in this work had the highest signal to noise ratio in the image, and regions further away from the center were approximated by employing polynomial curves to extend the anterior and posterior surfaces. However, extending the surfaces in this form could affect the method's reliability in estimating the tomography of the peripheral cornea.

Notable efforts at 3D segmentation of cornea images include a study by Robles et al. on images of mice corneas (Robles et al., 2014). Their technique was adapted from the graph cut techniques that had been developed for retinal OCT images. There was no discussion of issues of inter-image misalignment in their paper and their validation only considered the 2D segmentation step. Another group has carried out construction of a 3D surface using segmentation of SD OCT comprising multiple 2D images of

the cornea (Eichel et al., 2010). This group used peak detection and a generalized Hough transform to segment 2D images. The images used included both perpendicular and parallel sets with equal spacing in the two directions. The group then minimized the distance between the 2D cornea edges at the cross over points of the images to align the images and create a 3D reconstruction of the cornea. The technique was demonstrated on only 3 image sets from 3 healthy subjects and the results were not validated.

More work has been carried out on the registration of posterior segment OCT images to produce 3D maps of the retina. A commonly used method is to exploit blood vessels which cross the retina and can be seen on multiple 2D cross sections of the images (Kolar and Tasevsky, 2010) (Lin and Ju, 2010). The cornea and retina have a different structure. The cornea is avascular and healthy corneas do not contain any defining features other than their uniform shape. This means that techniques developed for retinal OCT images cannot be easily transferred to images for use on the cornea.

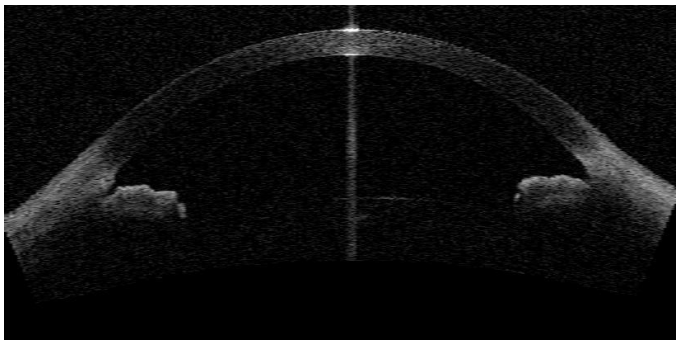

Fig. 1. An example TD OCT image of the anterior segment. The 3D images were made up of 16 2D images.

In this paper we propose a novel method for segmenting time domain OCT (TD OCT) images of the anterior segment. TD OCT produces lower resolution images compared to SD OCT but is currently the only widely used OCT technique to cover the entire anterior segment. An example 2D image to be segmented is show in Figure 1. In order to generate a 3D image of the cornea, 16 2D OCT images of the cornea were acquired. These were taken in a radial manner so all were expected to pass through the cornea's center. These images can individually be segmented on a 2D basis using the method described here. The challenge in segmenting these 2D images is the lower signal to noise regions that make the posterior surface hard to detect. We propose to use a shape term based on our successful detection of the anterior surface to overcome this problem, this is the first time segmentation using a shape term and graph theory segmentation has been used on anterior segment images. The challenge in producing reliable 3D segmentation is mainly caused by difficulties in alignment of 2D images. The possible involuntary eye movement could cause misalignment between 2D scans as illustrated in Figure 2, and make the resulting 3D surfaces unreliable. We propose to use genetic algorithms to solve this problem. The main advantage of GAs is their ability to globally minimize a function that may contain many local minima. They have been used in other image registration contexts with significant success (Chow et al., 2004; He and Narayana, 2002; Wang and Li, 2011).

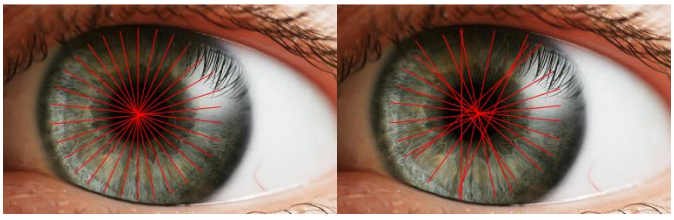

Fig. 2. Diagram showing the 3D scan pattern. Left image shows an ideal scan expected to achieve, right image illustrates a misaligned scan which often occurs in practice. Each red line represents a 2D image similar to the one shown in Figure 1.

The images for this study were all acquired from ocular healthy patients. For the 3D study artificial tears were instilled in eyes in order to obtain good quality images.

The remainder of the paper is structured as follows. Section II will present a novel 2D segmentation which uses graph theory and a shape constraint term to segment the images. Section III presents a novel approach to aligning segmented 2D images to produce a 3D map of the anterior segment. Section IV presents the validation methods used and the sources of images used in the study. Section V presents the results of the validation analysis. Section VI discusses the results and conclusions.

2. Method – 2D Segmentation

Our 2D segmentation algorithm consists of five major steps. Two surfaces are detected: the boundary between the corneal epithelium and air which we define the anterior surface and the boundary between the stroma and the corneal endothelium which we define as the posterior surface. First a pre-processing step is carried out to locate the iris. An initial segmentation of the anterior surface is carried out with the iris removed from the image. This segmentation is used to create a shape function. Final segmentation of the anterior and posterior surfaces is then carried out. Figure 3 illustrates these major steps. Each step will be discussed in more detail. Figure 4 shows the progress after each of the described steps.

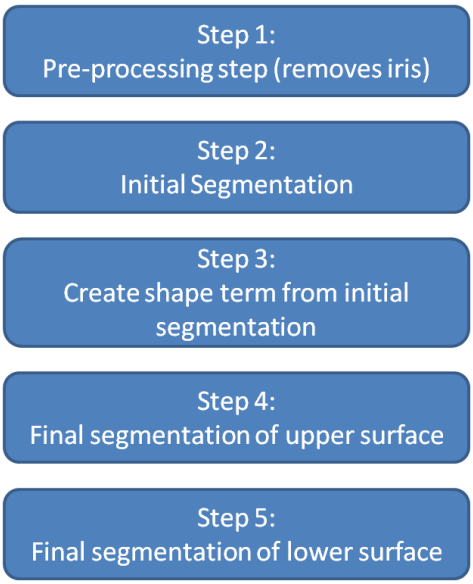

Fig. 3. Flow chart showing the steps of the 2D segmentation technique

2.1. Pre-processing Step

Anterior segment OCT images contain both the iris and the cornea. These are both structures that go across the image so our segmentation must distinguish between them. The first step in our segmentation program is therefore to identify the region that contains the iris to prevent it being incorrectly identified as the cornea. This is done by checking the mean intensity of the horizontal rows in the image. The iris will correspond to the row with be the maximum intensity since it is a flat horizontal structure. Once the iris is identified that region is removed from the image for the initial segmentation. In Figure 4 the image centre left shows the image after this step.

2.2. Initial Segmentation

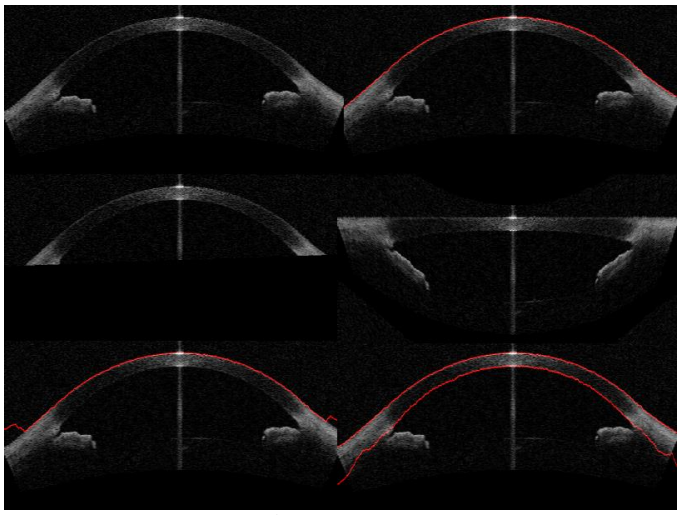

Fig. 4. Illustration of segmentation steps. Initial image is shown top left. The cropped image with the iris removed is shown centre left. The segmentation of the cropped image is show bottom left, note missing sections at either edge of image. Top right image shows final segmentation of anterior surface. Centre right image shows flattened image based on segmentation of anterior surface. Bottom right shows final segmentation of anterior and posterior surfaces.

The remaining part of the image is then segmented using graph theory. Each pixel of the image is regarded as a node of a graph which represents the image. Now the segmentation problem becomes to find the shortest path from the left to the right of the image. More specifically, the following energy term is used to define the weighting of each node on the image.

$$C_1(x,z) = w_1 * \frac{\partial I(x,z)}{\partial z} + w_2 * \frac{\partial I(x,z)}{\partial x}, \qquad (1)$$

where w_1 and w_2 are weighting coefficients, $\partial I(x,z)/\partial z$ is the vertical gradient of the image at point (x,z) and $\partial I(x,z)/\partial x$ is the horizontal gradient of the image. The gradient was calculated using the Matlab gradient function which calculates the gradient using a central difference approximation. The reason for using a combination of the two gradients is the curvature of the cornea. In the central region the vertical gradient is at correct orientation to find the boundary. For the horizontal gradient the weighting of the central quarter of the image was set to zero. As the cornea curves towards the edges of the image the cornea edge is orientated towards the corners of the image so using both horizontal and vertical gradient is important. w_1 was set to 1 across the image and w_2 was set to zero in the central region and 1 elsewhere. One potential variation would be to alter the values of w_1 and w_2 using an estimation of the shape of the cornea. Results of this idea were not included since tests varying these values found that the results of the segmentation were not strongly related to the values of the weighting coefficients. In Figure 4 the image bottom left corresponds to the result of this step.

2.3. Final Segmentation of the Anterior Boundary

When the iris is removed, parts of the sclera are also removed with it. In order to segment the full width of the image the segmentation is repeated over the original full image. The result of the previous segmentation is used to guide the segmentation to avoid false detection of the iris. This gives a new cost function of

$$C_2(x,z) = w_1 * \frac{\partial I(x,z)}{\partial z} + w_2 * \frac{\partial I(x,z)}{\partial x} + w_3 * \phi_a(x,z), \qquad (2)$$

where ϕ_a is a distance function each point corresponds to the distance to the line detected in the previous step. This encourages the line to follow the path of the previous segmentation but allows it to extend into regions that were not part of the previous image. The three weighting terms were kept equal in this step, $w_1 = 1$, $w_2 = 1$, and $w_3 = 1$. The image top right in

Figure 4 shows the segmentation at this stage.

2.4. Final Segmentation of Posterior Surface

The next step of the segmentation is to detect the posterior surface. This is harder to detect than the anterior surface since the edge is not as well defined on this boundary. In order to aid detection of this boundary two strategies were introduced, one was to flatten the cornea using the anterior surface and the other is to use a shape guiding term constructed from the anterior surface. Flattening the cornea in the image aids segmentation since graph theory segmentation favors straight lines over curved lines in segmentation. This is done by shifting each column in the image so the anterior surface previously detected becomes a straight line on the image. The flattened image is shown middle right in Figure 4.

To calculate the shape term the central corneal width is calculated using an established technique where peaks in the image are found (Ge et al., 2012). The corneal thickness on either side of the center increases. A quadratic term was used to make an estimate of the thickness at each point along the cornea. The estimated thickness was given by

$$ct(x) = ct_{central} + c_1(x - x_t)^2 + c_2 \mid x - x_t \mid, \tag{3}$$

where ct(x) is the estimated corneal thickness at point x, $ct_{central}$ is the central corneal thickness, x_t is the location of the centre of the cornea and c_1, c_2 are coefficients that determine the strength of the quadratic terms. The strength of these coefficients was determined by empirical testing. The values used where c_1 = 0.00033 and c_2 = 0.0077. This enabled the generation of an estimated location of the posterior surface. A distance function was generated and used to guide the segmentation of the posterior surface.

The cost function for the posterior surface is given by

$$C_3(x,z) = w_1 * \frac{-\partial I(x,z)}{\partial z} + w_2 * \frac{-\partial I_f(x,z)}{\partial z} + w_3 * \phi_p(x,z), \tag{4}$$

where w_1, w_2, w_3 are weighting functions to determine the strength of the different terms, $\partial I(x,z)/\partial z$ is the gradient in vertical direction and $\partial I_f(x,z)/\partial z$ is the gradient in the vertical direction after a median filter was applied to the image. This filter was used to reduce to effect of noise on the segmentation; the shape of the filter was a vertical line of 5 pixels. $\phi_p(x,z)$ is the shape term determined from the anterior surface through the method discussed above. The negative gradient is assumed as the posterior surface is a boundary from light to dark unlike the anterior surface. Horizontal gradient is no longer used since the cornea has been flattened. The strength of the weighting functions used was w_1 = 1, w_2 = 1, and w_3 = 0.5.

Figure 4 shows the progress of the segmentation following conduct of the steps discussed above.

The determination of the weighting coefficients for the different stages was carried out using a leave one out technique. A range of values was tested for each weighting term. For each of the 39 images the values of the coefficients that gave the best results for segmentation over the other 38 images was used. It was found that the same values were found to work best for all the different images. The values used for the coefficients are stated in each of the sections.

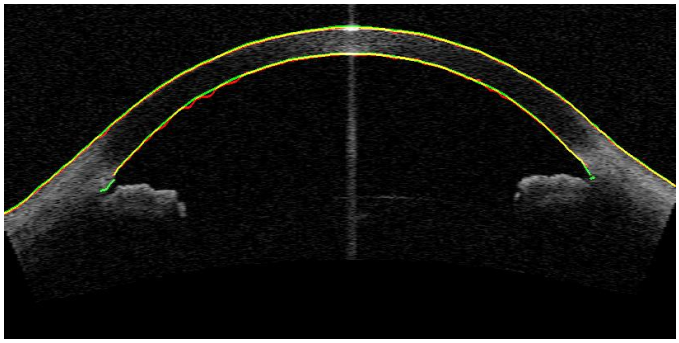

Fig. 5. Illustration showing automatic segmentation (red) and manual segmentation (green) on the example image. Where lines overlap the colors are mixed (yellow). The manual segmentation of the posterior boundary was only carried out up to the iris since the boundary is not well described beyond the iris.

2.5. Energy Minimization

After determining the weighting function $C_{1,2,3}(x,z)$ the shortest path for each function was found using the dynamic programming technique. This works by calculating the cumulative cost function for each point using the following expression

$$t(x,z)=\begin{cases}\infty & z<1, z>m \\ C(x,z) & x=1 \\ \min\limits_{p=z-3:z+3}\begin{pmatrix}t(x-1,p)+C(x-1,z-1)+C(x,z),\\ t(x-1,p)+C(x,z),\\ t(x-1,p)+C(x-1,z+1)+C(x,z)\end{pmatrix} & p=z-3\,or \\ & \mathrm{p}=z+3 \\ \min\limits_{p=z-2:z+2}\left(t(x-1,p)+C(x,z)\right) & otherwise\end{cases}, \tag{5}$$

where $t(x,z)$ is the cost to reach point (x,z), $C(x,z)$ is the weight function giving the cost at node (x,z), x is the x direction index, z is the z direction index and m is the image height. The cost function used depends on which surface is being found. The shortest paths for $C_{1,2,3}(x,z)$ defined in previous equations are all found using this method. This minimization method controls how steep a line can be found in the image. Each pixel can be connected to one of closest 7 pixels from the previous column. If it is one of the 5 closest only the values at the previous point are taken into account. If there has been a move of 3 pixels up or down then an additional cost is added from a point in the same column. The choice of an additional point from the previous column was made since the boundary is considered to pass through this point. This allows for steep lines to still be detected while preventing too much movement in the vertical direction without a cost penalty occurring. Only one point is found for each point on the x axis. Figure 5 displays the results of this segmentation on an image also containing manual segmentation results.

3. METHOD - 3D REGISTRATION

In order to generate a 3D surface from the 2D segmentation results a suitable method for alignment must be developed since errors may develop in 2D image position and orientation due to possible eye motion and incorrect camera positioning. Figure 6 shows an example image of the anterior surface generated when our alignment process is not used. The need for this registration step means that direct 3D segmentation is not practical.

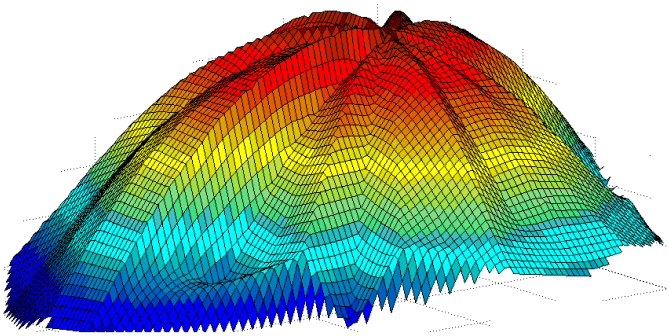

Fig.6. An example of a 3D anterior surface of the cornea generated before alignment process has taken place.

3.1. Identification of landmarks

In the 2D segmentation we have identified the anterior and posterior surfaces as well as an estimate of the location of the iris. In order to carry out a course alignment of 2D images, 3 points are identified on each image; the apex of the cornea and both junctions of the iris and cornea. The apex of the cornea can be identified by finding the point with the minimum z coordinate on the anterior surface, where z is the vertical axis on the image with the zero point at the top of the image. The two junction points can be identified as where the approximate iris location crosses the posterior surface, Figure 7. Once these three points are identified on all the images they can be used to align the images.

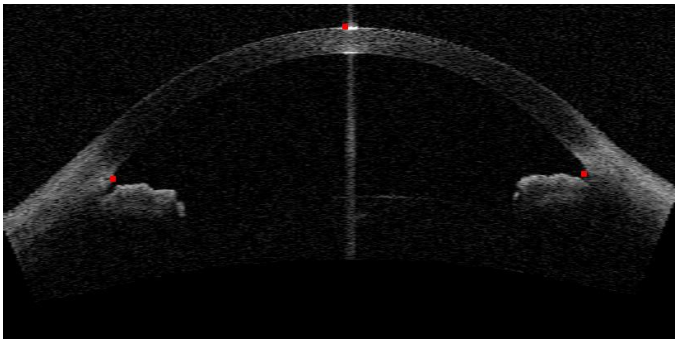

Fig.7. Illustration showing the landmark points identified as first step in alignment. The point in the centre of the image is the apex of the cornea. The points on the left and right of the image are the junction points where the iris and cornea meet.

The vertical distance from the apex of the cornea to the line connecting the points at the edge of the iris is used as a measure of the anterior chamber depth, which should remain constant or vary within very tight limits in 2D images taken for the same eye. Images that are not aligned with the center of the cornea will likely have a smaller depth. A linear relation between the anterior chamber depth and the distance between the image and the cornea's center was assumed due to the expected small values of the misalignment distances. A quadratic relation was tested but this was found to be less accurate than using the linear method. This is probably due to the errors in the calculation of the chamber depth which would be magnified when using a quadratic relation compared to a linear one. Further, a vertical displacement was implemented to each image based on the mean height of the two iris points on each image. These heights should be the same since the iris is a relatively flat structure, and hence any variations are assumed to result from the eye's rigid motion in the anterior-posterior direction. Finally any displacement in the horizontal plane of the image is eliminated by aligning the apex points on each image so they are all have the same x position.

3.2. Alignment

The results of the preliminary alignment were reasonable but still contained errors in alignment, which made it necessary to carry out a further step. It was decided to use genetic algorithms (GA) since it is a technique that is able to effectively minimise a function with many local minima. The results obtained when only the preliminary alignment was used are included in the analysis for comparison. GA is a technique with a trial and improvement basis, which can be used to minimize an energy function (David, 1989). With GA, a series of parameters are randomly initialized within a range. These solutions are ranked using a fitness function. New solutions are generated by combining the best solutions of each step as well as adding in a random element. This technique is good for finding a global minimum for demanding applications, where more conventional minimization techniques may end up finding only local minima. The challenge in using GA is the selection of a suitable energy function.

Zernike polynomials have been previously used to model the surface of the cornea (Iskander et al., 2001), defining it by the following expression

$$C(r,\theta) = \sum_{p=1}^{P} a_p Z_p(r,\theta) + \varepsilon , \qquad (6)$$

where $C(r,\theta)$ is a mathematical representation of the corneal surface, p is the polynomial ordering index, $Z_p(r,\theta)$ the pth order Zernike polynomial with associated coefficient a_p and ε is the experimental and modeling error.

A model cornea was created by fitting Zernike polynomials up to the fifth order to a surface generated from the preliminary step. This process created a smooth surface in the expected shape of the cornea. The mean distance between the surface generated from the images and this model surface was used as the energy function, which took the form:

$$E = \sum_{i=1:N} abs(z_i^{surface} - z_i^{zernike}) , \qquad (7)$$

where $z_i^{surface}$ is a point on the test surface, $z_i^{zernike}$ is a point with same x and y coordinates on the polynomial surface and N is the total number of points on the test surface. The points on the test surface were all points on the individual slices no smoothing or fitting was applied at this stage. GA was used to minimize this energy function over 64 parameters corresponding each of the 16 2D images being free to move in all 3 directions and rotate in the image plane.

Points on the same B scan were not allowed to move relative to each other. This means all points on each of these scans were always moved the same amount.

The Matlab implementation of the GA was used with a total population of 100, of which 4 are elite, 80 are crossover offspring and 16 are mutation offspring. Mutation offspring are produced by randomly generating a direction and step length that satisfies the boundary condition. Crossover offspring are created by taking a weighted average of the parents. The process was run until it showed no improvement over a period of 100 generations.

In order to improve the results the preliminary alignment discussed above was used as a constraint on the range of the parameters. The range of possible displacements and rotations for each image was limited to values that were close to the result of the preliminary alignment. The displacement in the x and y directions was limited to 20 pixels in either direction and a maximum rotation of 10 degrees was allowed. If much wider limits were used then this would reduce the effect of the preliminary alignment on the final result. Increasing these values would reduce the effect of the preliminary step, results are presented for alignment both with and without this preliminary step for comparison. Once the registration of the images was completed a 5th order Zernike polynomial was fit to the results in order to generate a surface including points not on the original slices. This was done separately to the anterior and posterior surfaces.

4. VALIDATION

A systematic approach was adopted to evaluate the performance of the proposed segmentation technique.

The automatic 2D segmentation technique was compared to the output of manual observers using three measures. The first measure is Dice Similarity Coefficient (DSC) which is a measure of what proportion of the segmentation is shared between the two images (Dice, 1945). DSC is defined by the following equation.

$$DSC = \frac{2|P \cap Q|}{|P| + |Q|} \qquad (8)$$

Where P and Q are the two segmentations to be compared, in this case the manual and automated segmentation results. DSC has a range between 0 and 1. The higher the DSC value, the more similar the two segmented regions are.

The second measure is the unsigned mean surface position error (MSPE) which is a measure of the distance between the boundaries from two different segmentation techniques at each point across the image.

Thirdly, the 95% Hausdorff distance which is a measure of the maximum distance between two matching points in the results of two different segmentation techniques (Huttenlocher et al., 1993). The Hausdorff distance from set A to set B is defined as

$$HD(A,B) = \max_{a \in A}[\min_{b \in B}(|a-b|)], \qquad (9)$$

where A and B are sets of boundary points from the two images to be compared. The 5% largest distances were removed then the maximum of HD(A,B) and HD(B,A) was determined for each image (Archip et al., 2007). This step was performed to remove the effect of a small number of badly located points from the analysis. Hausdorff distance is the measure of the misalignment of the worst point. Perfect alignment is represented by a Hausdorff distance of 0.

Three different automatic 2D segmentation methods were compared in the study, including our novel method, a previously published level set method (Williams et al., 2013) and the graph theory method without a shape term (which is equivalent to a previously published method (LaRocca et al., 2011)). Inter and intra observer differences were also compared. Our method without shape term differs from the method used by LaRocca et al. in the preprocessing steps used. The preprocessing steps used by that group were implemented but it was found the preprocessing steps used here worked better on our data set.

The validation of the 3D technique was carried out by comparing the results of segmentation of two different sets of images of the same eye. The mean difference between the anterior surfaces generated was used as a measure of similarity. This distance was calculated between the surfaces after the Zernike polynomial had been fitted to generate smooth surfaces.

For the 2D segmentation work, 39 anterior segment OCT images were taken through the center of the cornea from healthy eyes (one per subject). The study was approved by the institutional review board and undertaken while following the tenets of the Helsinki Declaration. The images were acquired by the Visante AS-OCT system at the Wenzhou Medical University, China. The Visante system is a time domain system that uses 1,300nm infrared light to obtain cross-sectional images of the anterior segment with a scanning rate of 2,000 axial scans per second. Each B scan image contains 256 A-scans in 16mm with 1024 points per A scan to a depth of 8mm. The images have a transverse resolution of 60μm and an axial resolution of 18μm. These images were manually segmented by two expert ophthalmologists (FB and MS) marking on the locations of the anterior and posterior boundaries.

In validating the 3D segmentation method, images of 17 eyes were acquired using the Visante AS-OCT system. These were taken at the Western University of Health Sciences, California, United States. A total of 17 healthy eyes were imaged for this study. 5 eyes were from volunteers who had only one eye imaged and 12 eyes were from volunteers who had images taken of both eyes. For each eye, two 3D images were recorded. Two sets of images were taken per eye with a short period of rest to enable a repeatability test to be carried out of our 3D alignment technique. Alignment was carried out using three techniques,

namely the initial identification of landmarks step, using GA without the initial step and using both GA and the initial step. These techniques were compared to assess their relative effectiveness.

Statistics calculations were made using SPSS version 20 (IBM, Armonk, NY, USA).

5. RESULTS

5.1. 2D Segmentation

Table 1 shows the results of comparison between manual segmentation and a number of automated methods. The methods considered include that presented here and two previously used techniques, in addition to manual segmentation by a second observer. Our newly developed method achieved a DSC value of 0.962, compared to 0.966 for inter observer difference. Carrying an ANOVA test on the DSC results using SPSS it was found that there were significant differences between the four methods. Post hoc analysis found significant difference between our novel graph theory technique and level set based methods ($p<0.05$) but not between the novel graph theory and inter observer comparison ($p=0.98$). This shows that our newly developed method performs better than previously reported techniques and is equally as good as manual segmentation. While the anterior surface was found just as well with or without the shape term the posterior surface could not be correctly identified without use of the shape term.

It is worth noting that the Graph Theory with no shape is very similar to the method shown by LaRocca et al. in (LaRocca et al., 2011). They only presented data of the central region which is the region with the best signal to noise ratio. In this paper we have calculated the results of this method over the entire posterior surface and so have not been able to achieve results as accurate achieved by the original authors of the paper.

Carrying out similar statistical analysis for the other measures used produced similar results. When looking at the anterior surface MSPE there was no significant difference between any of the techniques. For the posterior MSPE and Hausdorff distance measures a significant improvement compared to previous level set and graph cut methods was shown and again no significant difference when compared to manual segmentation. Our new method achieved a MSPE of 1.10 pixels on the anterior surface and 1.75 pixels on the posterior surface. A 95% Hausdorff value of 4.1 pixels was achieved. The lack of significant improvement on segmentation of the anterior surface is probably due to the fact that this is the easiest surface to find. This meant there was little difference between the methods since they were all able to detect the surface well.

TABLE I

COMPARISON WITH MANUAL OBSERVER FOR THREE DIFFERENT AUTOMATIC SEGMENTATION TECHNIQUES AND MANUAL SEGMENTATION BY ANOTHER OBSERVER

Segmentation Technique	Our proposed Graph Theory Technique	Graph Theory no shape	Level Set	Inter Observer
DSC				
Mean	0.962	0.668	0.919	0.966
Standard Deviation	0.009	0.125	0.026	0.007
MSPE Anterior				
Mean **(**pixels)	1.10	1.10	1.64	1.31
Standard Deviation **(**pixels)	0.33	0.33	0.52	0.53
MSPE Posterior				
Mean **(**pixels)	1.75	17.3	3.90	1.78

Standard Deviation (pixels)	0.60	4.67	1.81	0.67
95% HD				
Mean (pixels)	4.10	28.5	9.50	3.58
Standard Deviation (pixels)	1.61	2.9	4.33	0.96

5.2. 3D Alignment

Results for these comparisons are shown in Table 2. This shows the mean difference between the anterior surfaces on two different images of the same eye. For our best method, the GA with pre alignment from landmark points, the mean difference was 1.77 pixels. This is a substantial improvement on results achieved without GA. Looking at the mean difference measurement we can see that the method using genetic algorithms performs substantially better than when no registration step is carried out. The GA methods achieve much better results compared to the initialisation step alone. There was a further improvement when using the GA with initialisation as compared to GA when no initialisation was used.

The mean difference for the best method was 1.77 pixels, when looking at the 2D segmentation the difference between our segmentation and the manual observer was 1.10 pixels. This implies that there is a possible error in segmentation of around 1 pixel from the segmentation which would be present in the alignment results. The error in the alignment has three contributions, errors from the imaging process, errors in the segmentation and errors due to the alignment process itself. It would therefore be unlikely to obtain results with a better reproducibility than the error in the segmentation.

TABLE II

REPEATABILITY MEASUREMENTS TAKEN USING A DATA SET OF 17 EYES. THREE DIFFERENT REGISTRATION TECHNIQUES ARE COMPARED

Method	Mean Difference	Standard Deviation
No Registration	51.2	22.7
Preliminary step only	14.1	3.2
GA, without preliminary step	2.52	0.64
GA, with preliminary step (our proposed method)	1.77	0.59

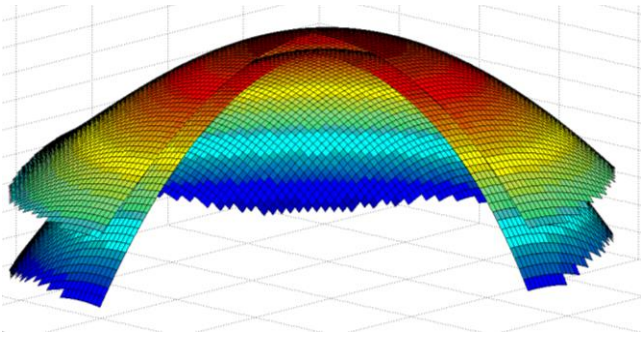

Fig. 8. Example of 3D surfaces generated by the process. Both anterior and posterior surfaces are shown. A quarter of the image has been cut away so both surfaces can be seen.

6. Discussion and conclusion

A novel method for the segmentation and alignment of anterior segment OCT images has been developed. The 2D segmentation has been shown to segment images as accurately as manual segmentation when compared to two different manual observers. The 3D alignment technique has shown good repeatability. There have been no previous studies presenting quantitative validation of the reconstruction of a 3D surface using human anterior segment OCT images. Eichel et al present a method for segmenting and aligning 3D SDOCT images (Eichel et al., 2010). Their paper carries out validation tests for the 2D segmentation process but they only have data from 3 eyes for their 3D work so do not present any validation of the reliability of their technique.

The method presented here has shown that accurate segmentation and alignment of anterior segment images taken using time domain OCT images can be achieved. TD OCT system has been used since these are a widely available imaging technology that is able to produce images across the entire anterior segment. Many commercial SD OCT imaging systems have shorter penetration depths, due to choice of wavelength used, and are only capable of imaging part of the anterior segment, several groups have custom built SD OCT devices capable of achieving images with a larger penetration depth (Du et al., 2012; Karnowski et al., 2011; Ortiz et al., 2013). The Tomey Casia system is the only commercial SD OCT system able to image the entire anterior segment.

The segmentation and alignment method described here is a generic tool that will be transferable to SD OCT images. Due to the superior resolution of SD OCT we expect the segmentation performance of the tools presented here to be better than what was obtained in present study using TD OCT.

This is the first time to our knowledge that a 3D reconstruction system has been developed and validated on OCT images of the anterior segment of human eyes. By creating a segmentation method that can produce a surface map of two surfaces covering the entire area of the cornea we have developed a tool that can be used by clinicians to help diagnosis. The structure and the shape of the anterior segment is an important measure of a number of different pathologies of the eye including glaucoma and keratoconus. Producing maps of the anterior segment like this will allow us to produce patent specific biomechanical modals of the human cornea.

Future improvements to this technique will involve investigating how well the segmentation and alignment can cope with the examination of diseased eyes. As devices improve their ability of imaging further segmentation of individual layers of cornea, particularly the epithelium will be a valuable addition.

In conclusion a novel method has been developed for the segmentation and alignment of 3D anterior segment OCT images. This method has been shown to perform better than previously used techniques when compared to manual segmentation. There is potential for this method to become a valuable tool to provide accurate and reliable measurements of the anterior segment geometry for future clinical and non-clinical applications.

REFERENCES

Archip, N., Clatz, O., Whalen, S., Kacher, D., Fedorov, A., Kot, A., Chrisochoides, N., Jolesz, F., Golby, A., Black, P.M., Warfield, S.K., 2007. Non-rigid alignment of pre-operative MRI, fMRI, and DT-MRI with intra-operative MRI for enhanced visualization and navigation in image-guided neurosurgery. NeuroImage 35, 609-624.

Chow, C.K., Tsui, H.T., Lee, T., 2004. Surface registration using a dynamic genetic algorithm. Pattern Recognition 37, 105-117.

David, E.G., 1989. Genetic Algorithms in Search, Optimization and Machine Learning. Addison-Wesley Longman Publishing Co., Inc.

Dice, L.R., 1945. Measures of the Amount of Ecologic Association Between Species. Ecology 26, 297-302.

Dijkstra, E.W., 1959. A note on two problems in connexion with graphs. Numerische Mathematik 1, 269-271.

Du, C., Shen, M., Li, M., Zhu, D., Wang, M.R., Wang, J., 2012. Anterior segment biometry during accommodation imaged with ultralong scan depth optical coherence tomography. Ophthalmology 119, 2479-2485.

Eichel, J.A., Bizheva, K.K., Clausi, D.A., Fieguth, P.W., 2010. Automated 3D reconstruction and segmentation from optical coherence tomography.

Ge, L., Shen, M., Tao, A., Wang, J., Dou, G., Lu, F., 2012. Automatic segmentation of the central epithelium imaged with three optical coherence tomography devices. Eye and Contact Lens 38, 150-157.

Hall, R.C., Mohamed, F.K., Htoon, H.M., Tan, D.T., Mehta, J.S., 2011. Laser in situ keratomileusis flap measurements: Comparison between observers and between spectral-domain and time-domain anterior segment optical coherence tomography. Journal of Cataract and Refractive Surgery 37, 544-551.

He, R., Narayana, P.A., 2002. Global optimization of mutual information: Application to three-dimensional retrospective registration of magnetic resonance images. Computerized Medical Imaging and Graphics 26, 277-292.

Huttenlocher, D.P., Klanderman, G.A., Rucklidge, W.J., 1993. Comparing images using the Hausdorff distance. IEEE Transactions on Pattern Analysis and Machine Intelligence 15, 850-863.

Iskander, D.R., Collins, M.J., Davis, B., 2001. Optimal modeling of corneal surfaces with Zernike polynomials. IEEE Transactions on Biomedical Engineering 48, 87-95.

Kaluzy, B.J., Kałuzny, J.J., Szkulmowska, A., Gorczyńska, I., Szkulmowski, M., Bajraszewski, T., Wojtkowski, M., Targowski, P., 2006. Spectral optical coherence tomography: A novel technique for cornea imaging. Cornea 25, 960-965.

Karnowski, K., Kaluzny, B.J., Szkulmowski, M., Gora, M., Wojtkowski, M., 2011. Corneal topography with high-speed swept source OCT in clinical examination. Biomedical Optics Express 2, 2709-2720.

Kolar, R., Tasevsky, P., 2010. Registration of 3D retinal optical coherence tomography data and 2D fundus images, pp. 72-82.

Konstantopoulos, A., Kuo, J., Anderson, D., Hossain, P., 2008. Assessment of the use of anterior segment optical coherence tomography in microbial keratitis. American Journal of Ophthalmology 146, 534-542.e532.

LaRocca, F., Chiu, S.J., McNabb, R.P., Kuo, A.N., Izatt, J.A., Farsiu, S., 2011. Robust automatic segmentation of corneal layer boundaries in SDOCT images using graph theory and dynamic programming. Biomedical Optics Express 2, 1524-1538.

Lin, L., Ju, Y., 2010. Automatic extraction of the anterior chamber contour in OCT images, 2nd International Symposium on Information Science and Engineering, ISISE 2009, pp. 423-426.

Liu, S., Yu, M., Ye, C., Lam, D.S.C., Leung, C.K.S., 2011. Anterior chamber angle imaging with swept-source optical coherence tomography: An investigation on variability of angle measurement. Investigative Ophthalmology and Visual Science 52, 8598-8603.

Ortiz, S., Pérez-Merino, P., Durán, S., Velasco-Ocana, M., Birkenfeld, J., de Castro, A., Jiménez-Alfaro, I., Marcos, S., 2013. Full OCT anterior segment biometry: An application in cataract surgery. Biomedical Optics Express 4, 387-396.

Reinstein, D.Z., Gobbe, M., Archer, T.J., 2012. Anterior segment biometry: A study and review of resolution and repeatability data. Journal of Refractive Surgery 28, 509-520.

Robles, V.A., Antony, B.J., Koehn, D.R., Anderson, M.G., Garvin, M.K., 2014. 3D graph-based automated segmentation of corneal layers in anterior-segment optical coherence tomography images of mice, Progress in Biomedical Optics and Imaging - Proceedings of SPIE.

Sakata, L.M., Lavanya, R., Friedman, D.S., Aung, H.T., Gao, H., Kumar, R.S., Foster, P.J., Aung, T., 2008. Comparison of gonioscopy and anterior segment ocular coherence tomography in detecting angle closure in different quadrants of the anterior chamber angle. Ophthalmology 115, 769-774.

Shen, M., Cui, L., Li, M., Zhu, D., Wang, M.R., Wang, J., 2011. Extended scan depth optical coherence tomography for evaluating ocular surface shape. Journal of Biomedical Optics 16.

Swanson, E.A., Izatt, J.A., Hee, M.R., Huang, D., Lin, C.P., Schuman, J.S., Puliafito, C.A., Fujimoto, J.G., 1993. In vivo retinal imaging by optical coherence tomography. Optics Letters 18, 1864-1866.

Tian, J., Marziliano, P., Baskaran, M., Wong, H.T., Aung, T., 2011. Automatic anterior chamber angle assessment for HD-OCT images. IEEE Transactions on Biomedical Engineering 58, 3242-3249.

Wang, Q., Li, X., 2011. Application of improved genetic algorithm in practical medical image registration. International Journal of Digital Content Technology and its Applications 5, 60-67.

Williams, D., Zheng, Y., Bao, F., Elsheikh, A., 2013. Automatic segmentation of anterior segment optical coherence tomography images. Journal of Biomedical Optics 18, 056003-056003.

Williams, D., Zheng, Y., Bao, F., Elsheikh, A., 2015. Fast segmentation of anterior segment optical coherence tomography images using graph cut. Eye and Vision 2, 1.